
HAMAMATSU PRESENTS
ANALYTICAL TALKS
WATCH NOW

Received: 16 July 2021 | Revised: 14 October 2021 | Accepted: 27 October 2021

DOI: 10.1111/jmi.13072

Journal of Microscopy RMS

THEMED ISSUE ARTICLE

Workflow for high-resolution phase segmentation of cement clinker from combined BSE image and EDX spectral data

Mingze Jiang[1] | **Christiane Rößler Dr. rer. nat**[2] | **Eva Wellmann**[1] | **Jop Klaver Dr. rer. nat**[3] | **Florian Kleiner**[2] | **Joyce Schmatz Dr. rer. nat.**[1]

[1] MaP - Microstructure and Pores GmbH, Aachen, Nordrhein-Westfalen, Germany

[2] F. A. Finger-Institute for Building Material Science, Bauhaus-Universität Weimar, Weimar, Thüringen, Germany (Email: christiane.roessler@uni-weimar.de)

[3] RWTH Aachen University, Aachen, Nordrhein-Westfalen, Germany

Correspondence
Florian Kleiner, F. A. Finger-Institute for Building Material Science, Coudrystraße 11A, 99423 Weimar, Bauhaus-Universität Weimar, Coudrystraße 11A, 99423 Weimar, Thüringen, Germany.
Email: florian.kleiner@uni-weimar.de

Funding information
Bundesministerium für Wirtschaft und Energie, Grant/Award Number: ZF4144918CL8

Abstract

Burning of clinker is the most influencing step of cement quality during the production process. Appropriate characterisation for quality control and decision-making is therefore the critical point to maintain a stable production but also for the development of alternative cements. Scanning electron microscopy (SEM) in combination with energy dispersive X-ray spectroscopy (EDX) delivers spatially resolved phase and chemical information for cement clinker. This data can be used to quantify phase fractions and chemical composition of identified phases. The contribution aims to provide an overview of phase fraction quantification by semi-automatic phase segmentation using high-resolution backscattered electron (BSE) images and lower-resolved EDX element maps. Therefore, a tool for image analysis was developed that uses state-of-the-art algorithms for pixel-wise image segmentation and labelling in combination with a decision tree that allows searching for specific clinker phases. Results show that this tool can be applied to segment sub-micron scale clinker phases and to get a quantification of all phase fractions. In addition, statistical evaluation of the data is implemented within the tool to reveal whether the imaged area is representative for all clinker phases.

KEYWORDS
cement clinker, image segmentation, EDX, superpixel

1 | INTRODUCTION

SEM-EDX has been used for decades to image and analyse cements.[1–6] The challenge of SEM-EDX analysis for cement-based materials is the small size of the phases as well as the wide variety of elements contained in these phases. Portland cement clinker consists of seven major phases: alite (impure form of Ca_3SiO_5) belite (impure form of Ca_2SiO_4) C_3A*[1] (cubic or orthorhombic polymorph, impure form of $Ca_3Al_2O_6$), C_4AF (solid solution with variable Fe_2O_3/Al_2O_3), periclase (MgO), free lime (CaO) and alkali sulphates (arcanite, K_2SO_4 or other).

Existing, highly specialised imaging systems, for example the QEMSCAN[7,8] or the Mineral Liberation System,[9] were developed to ensure efficient usage of the state-of-the-art imaging technologies also in industrial applications.

[1] Cement chemist notation: C - CaO, S - SiO_2, A - Al_2O_3, F - Fe_2O_3, M - MgO, K - K_2O, N - Na_2O, $ - SO_4

High-quality spectral data from EDX is used to segment and identify the different mineral phases automatically. However, applying the method to fine-grained materials (grain size $< 1\,\mu$m) remains a challenge due to insufficient spatial resolution, caused by the large size of the interaction volume where X-rays are emitted from.

The common approach to increase SEM imaging resolution is to reduce the acceleration voltage of the electron beam.[10] This has led to the field of low voltage electron microscopy with ultra-high-resolution for electron imaging. Depending on the material, a resolution down to 0.5–1 nm is achievable by now.[10] Chemically heterogeneous materials such as Portland cement require not only high-resolution imaging but also high-resolution EDX analysis. The factor that limits the resolution of EDX analysis is that heavy elements such as iron and titanium should be included in the analysis. Therefore, the minimum excitation energy needed is 7 keV (using X-ray L-lines for Fe and Ti), which still leads to a much lower EDX resolution as compared to the resolution of SEM imaging. As a result, a common approach is to combine the high-resolution BSE-SEM images with EDX mapping data aiming to improve the resolution of the EDX mapping data.[11]

A specific workflow together with an analysis tool is presented here that allows obtaining high-resolution phase maps from cement clinkers including quantification of phase fractions and representative element area (REA) analysis. The workflow comprises five steps as outlined in Figure 1: (1) acquisition of high-resolution BSE images and EDX mappings, (2) segmentation of combined BSE-EDX map into regions using superpixel algorithm, (3) adaptable decision tree that searches for clinker phases, (4) creating phase map and option to use a manual element intensity thresholding tool to improve the result and (5) REA analysis for individual clinker phases.

Standard image segmentation algorithms rely on thresholding and watershed algorithms,[12] which can be applied to grayscale images (e.g. BSE images) or single-channel arrays (e.g. EDX count arrays of a single element). However, they are not able to segment phases by taking into account EDX information from all relevant elements at the same time. Georget et al. (2021)[11] used a simple linear iterative cluster (SLIC[13]) segmentation algorithm to generate superpixels based on a RGB composite map, which combines three selected elemental EDX count arrays (e.g. red = Si, green = Al, blue = Ca). The superpixel segmentation partitions the image into subareas/regions while preserving image boundaries, that is, one subarea/region does not extend across two different objects/phases. SLIC is a cluster-based algorithm, which first initialises k cluster centres on a regular grid. Then, each pixel is associated with the nearest cluster centre whose search region overlaps its location according to colour similarity. After initialisation, a recursive update of cluster centres and pixels of each cluster will be performed until convergence. This approach has two drawbacks: (1) It can only segment phases using up to three elements. For example, it cannot consider all available EDX information. (2) The number of generated superpixels k must be defined beforehand and must be larger than the number of grains within the map. Because the number of phases in a map is difficult to predict, many superpixels should be generated to make sure, that no superpixel includes two different phases. However, the more superpixels are generated, the smaller each superpixel becomes. However, a relatively small superpixel may not contain sufficient amount of element intensity information, especially using short EDX scanning times.

With this contribution, we propose a novel segmentation algorithm based on edge detection and distance transform (DT) watershed, which can create regions with similar properties (superpixel) in BSE and EDX maps. We developed a semi-automatic tool based on decision trees and element threshold to enable fast phase class labelling. The obtained phase maps can be used for characterisation of various cement types and as ground truth for further machine learning-based automatic phase classification.

2 | MATERIALS AND METHODS

2.1 | Cement clinker

Portland cement clinker (type CEM I according to DIN/EN 197-1) obtained from an industrial process has been used for this investigation. The chemical composition of the clinker as determined by chemical analysis (inductively coupled plasma – optical emission spectroscopy) is given in wt.% as follows: 21.5 SiO_2, 5.8 Al_2O_3, 0.3 TiO_2, 3.1 Fe_2O_3, 65.6 CaO, 2.0 MgO, 1.1 K_2O, 0.1 Na_2O, 0.6 SO_3 and 0.1 P_2O_5.

2.2 | Sample preparation and imaging protocol

The sample material was a CEM I clinker, which was ground to a mean particle size of 25 μm. From this powder, tablets were pressed with an approximate diameter of 12 mm and a height of approximately 2–3 mm. This procedure ensures the homogeneity of the sample and maximum representativeness of the sample phase fractions. The tablets were embedded in epoxy resin using vacuum pressure impregnation. Polishing of the surfaces was carried out using oil-based diamond pastes with a

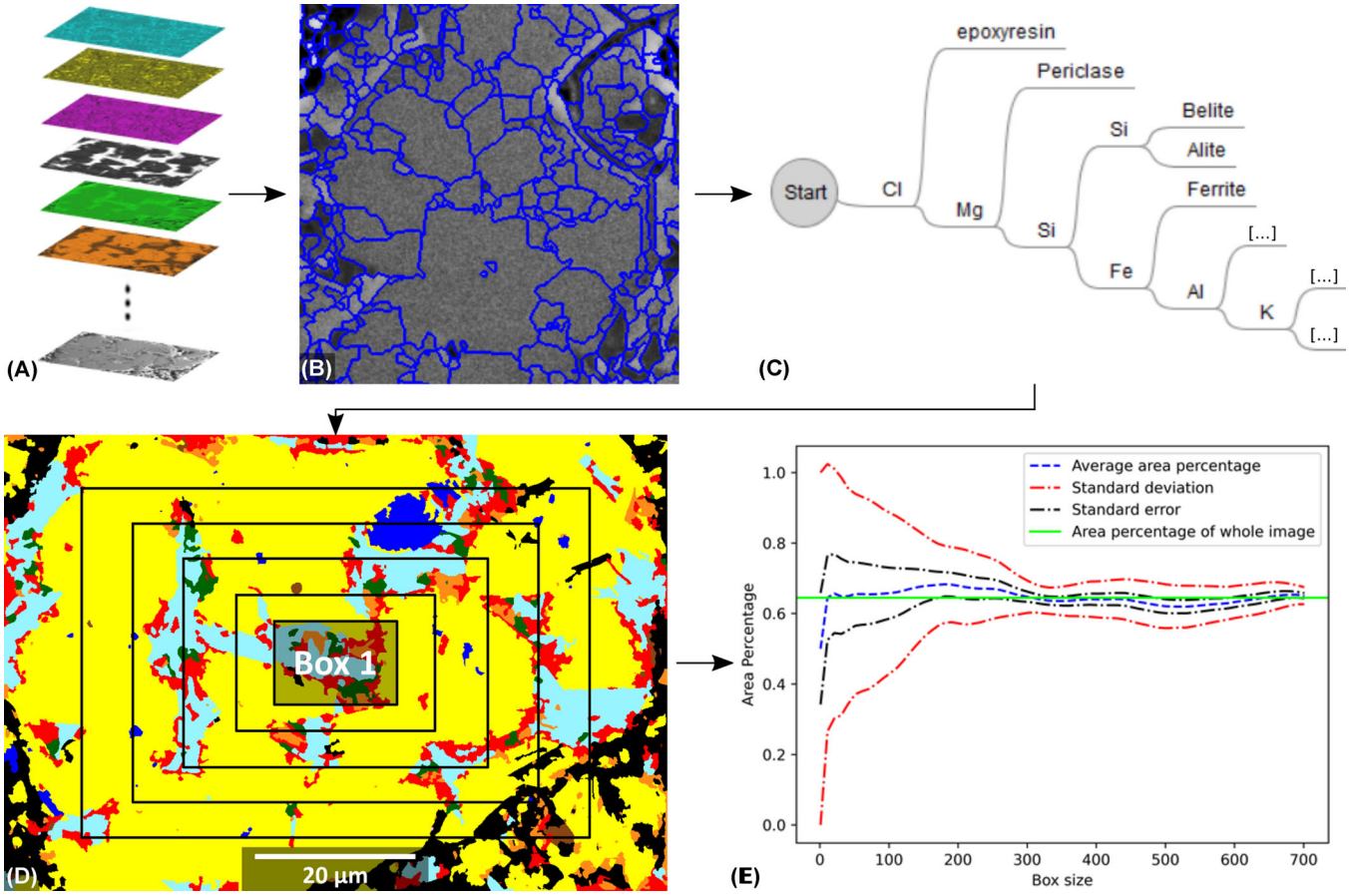

FIGURE 1 Workflow of the tool. (A) BSE/EDX hypermaps, (B) superpixel segmentation based on hypermaps overlaying a BSE image, (C) decision tree, (D) phase map overlayed by REA box calculation, (E) REA analysis for alite

decreasing particle size of 15, 9, 3, 1 and ¼ μm, respectively. To reduce the number of scratches and to further clean the surface, argon-broad ion beam (TIC 3X, Leica, Germany) etching was applied. The sample surface was tilted to an angle of 20° relative to the ion beams and a beam voltage of 4 kV was applied for 20 min on the rotating sample surface.

For the SEM-EDX analyses the samples were coated with a layer of approximately 10 nm carbon. The SEM-EDX analyses were performed with a Helios G4 UX (ThermofisherScientific, USA) including an EDX Detector (X-MAX 80, Oxford Instruments, UK). The SEM acceleration voltage was 12 kV and the EDX maps were acquired using the Aztec (Oxford Instruments, UK) software. The resolution of the acquired EDX maps is 0.08 μm/pixel. Resolution of the BSE image was 0.04 μm/pixel. The acquisition time for EDX element distribution maps was set as such that sufficient X-ray counts were detected (200–250 million counts per image at 12 kV and 0.8 nA) to distinguish alite and belite in the Si map and to distinguish orthorhombic and cubic C_3A using the combined Na and K map.

3 | RESULTS

3.1 | BSE and EDX image segmentation using a superpixel algorithm

In Figure 2, the results of a combination of segmentation algorithms are illustrated. Furthermore, the EDX element map (Figure 2A, here exemplarily the Al map) and the BSE image (Figure 2B) are shown. As the BSE segmentation was not sufficient to determine the exact phase boundaries of belite and C_3A, both BSE and Al segmentations were combined. The DT method was applied using the following steps: (1) detection of edges on BSE images and EDX element maps, (2) combining all edge maps into one single edge map, (3) generating a distance map by performing DT on the combined edge map, (4) computing superpixel by running a watershed algorithm on the distance map. After superpixel/regions were generated, each of these regions was treated as a homogeneous particle and was annotated to a corresponding class, which could be solved with the use of automatic machine learning classification algorithms such as random forest,[14] k-nearest neighbours[14]

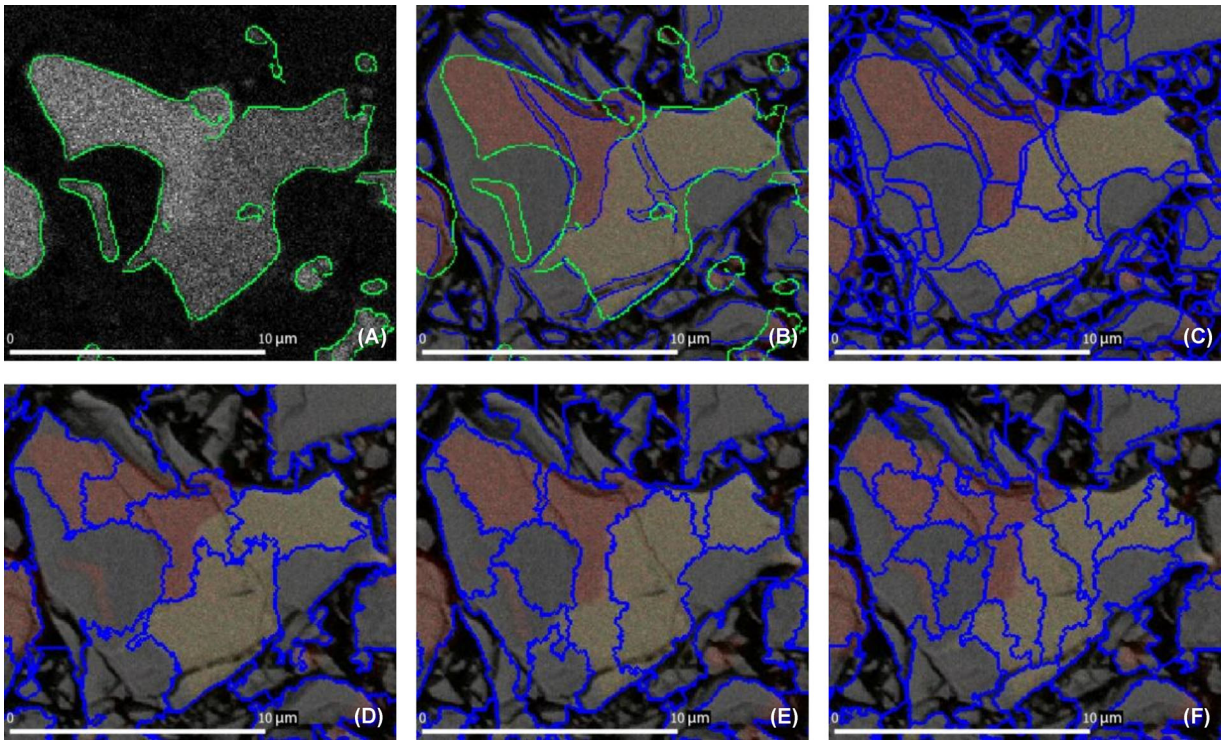

FIGURE 2 Superpixel segmentation, the background is a BSE image covered with a 50% transparent composite RGB image (red = Al, blue = Fe, green = Si). (A) Edge detection on Al map; (B) combined edge detection of BSE and Al map; (C) DT watershed result based on B (red = C_3A, yellowish grey = C_4AF, dark grey = belite); (D), (E), (F) SLIC segmentation with different amount of SLIC-superpixels per area (D < E < F)

or neural network.[15] However, machine learning algorithms require a large amount of training data/labelled data and to generate these data sets it is very time consuming, even with a state-of-the-art manual labelling tool.[16,17]

Results in Figure 2C and D compare the superpixels extracted by DT watershed as well as by the popular SLIC algorithm.[11] Both algorithms can capture most of the details in the background image. However, SLIC cannot detect the boundaries of some obfuscated phases, even after combining BSE and EDX into a composite RGB image, because the EDX data is often very noisy and the value differences are much smaller than the grey values within the BSE image. Besides that, as shown in Figure 2D and E, the set amount of SLIC-superpixels per area highly affects the result of the segmentation. Increasing the number of superpixels will not assure a better segmentation result. In contrast, DT watershed can extract most of the boundaries without a predefined superpixel size or amount (Figure 2C). Intuitively, DT watershed generates a segmentation which, according to visual inspection, outperforms the SLIC segmentation.

3.2 | Decision tree and manual thresholding

The identification of phases for the identified superpixel areas was done using a decision tree as shown in Figure 1. The decision tree allows searching for individual clinker phases using several element distribution maps. Decision trees for various types of cements (CEM I, calcium aluminate, calcium sulphoaluminate etc.) or other materials can be created and applied. Modifying the decision tree allows, for example, to search for Na- and K-rich C_3A using the Al, Na, K map. If the combined Na and K content of C_3A is above approximately 1.0 wt.% the orthorhombic polymorph is expected, below this threshold the cubic polymorph is prevailing.[1]

In a similar manner, the decision tree can be modified to search for other clinker phases like for example Ti-rich C_4AF.

Figure 3C and F shows two clinker phase maps that were obtained by using two different decision trees. For example, the K and Na element distribution maps were used to discriminate between the alkali rich and alkali poor C_3A

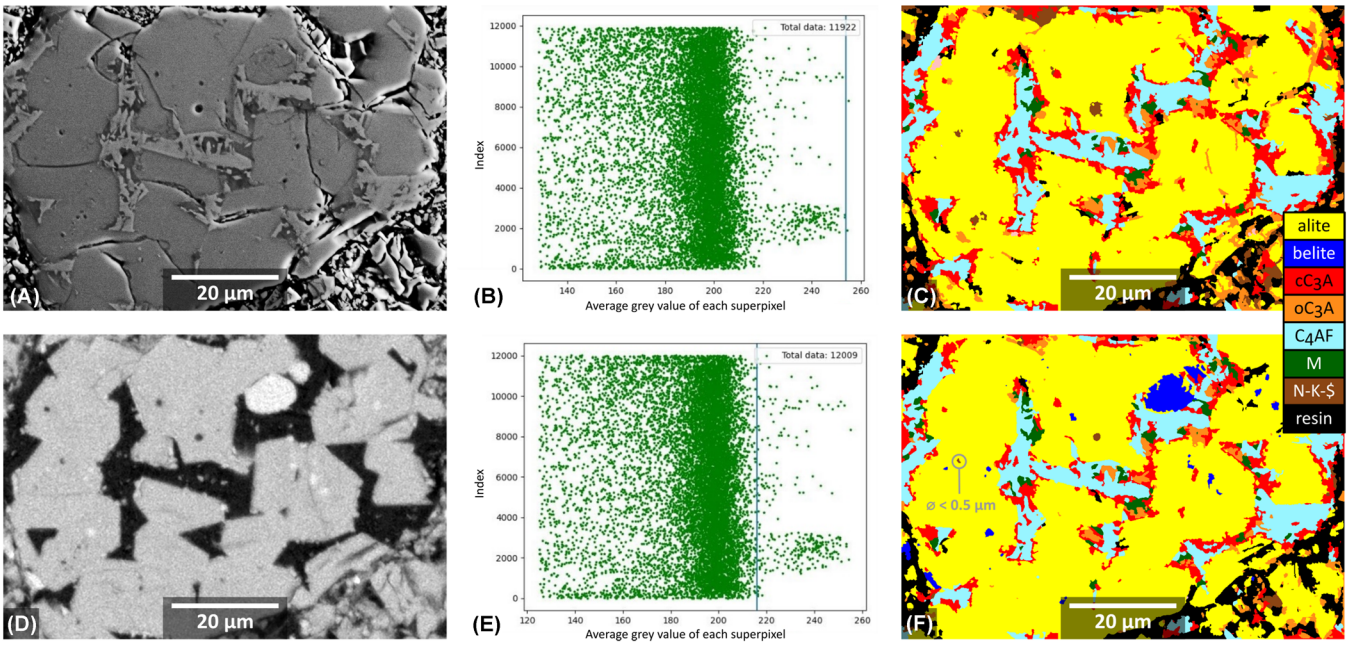

FIGURE 3 BSE image (A) and Si element distribution map (D) of a CEM I clinker. (B), (E) Intensities (*x*-axis) of superpixels in the Si map plotted against the index of superpixels. (D) Manual threshold in Si intensity map set to differentiate belite. (C), (F) Final phase maps without and with manually set threshold (C and F, respectively) as illustrated in E

(Figure 3F). The smallest feature size segmented in Figure 3C and F are belite inclusions in alite with a phase diameter of approximately 0.5 μm, which is in accordance to the Nyquist criterion.

To further support the phase identification, the tool allows users to manually adjust thresholds within the element distribution maps. As shown in Figure 3C–F the manual thresholding allows to separate belite (blue area in Figure 3F) from alite.

3.3 | Statistical evaluation (REA analysis)

Additionally, the developed software tool includes the possibility to determine a statistical evaluation if the analysed area is representative to quantify phase fractions (RAE analysis). In general, it plots the fractions of the different phases versus the image area, when the fractions do not vary significantly beyond a certain image area it can be inferred that the REA is reached. The user has the option to choose between a box counting and a statistical method.[18,19] The box counting method starts from a given box and is calculated by increasing the number of boxes or the box size until the actual image size is reached. In the statistical method the image is divided into non-overlapping boxes that are randomly selected, phase fractions are cumulated without resampling and plotted versus total box size.[20] This method is helpful when the phase fractions are spatially clustered for example due to preferential layering or grain size sorting. The results are plotted in a graph with average area percentage, standard deviation, standard error as well as area percentage of the whole image (Figure 1).

4 | CONCLUSIONS

The results presented here reveal that the developed tool performs high-resolution phase segmentation using BSE images and EDX mapping data. It was shown that a feature size of 0.5 μm diameter could be resolved by this analysis (Figure 3F). The used combination of superpixel image segmentation, decision tree-based phase search and the element intensity threshold tool allows to discriminate not only major cement clinker phases but also to search for specific phases such as orthorhombic and cubic C_3A, alkali sulphates etc. The determined phase fractions can further be used for clinker characterisation and to verify standard characterisation methods such as X-ray powder diffraction analysis of cements. Also, the tool, particularly the decision tree, can be adapted to analyse other composite materials such as rocks.

Ultimately, the tool provides an easy way to obtain phase distribution maps that can be used as ground truth for further machine learning-based image analysis.

The prerequisite for successful application of the tool is that the analysed BSE and EDX data are recorded with adequate resolution and sufficient number of X-ray counts.

Analysis of even smaller particles/inclusions contained in cement clinker and other materials can be achieved if for example more efficient EDX detectors are used and the number respectively size of the superpixels is decreased.

The tool is flexible and user-friendly and provides a multi-layer image viewing graphical interface. This interface can be used to manually design other decision-trees for new materials and to directly observe the corresponding phase masks on the BSE image. RAE analysis is also implemented in the interface

The next development step of the tool will implement an automatic output of the chemical composition of the segmented phases. The tool can be acquired by MaP GmbH or clinker analyses can be carried out upon request.

ACKNOWLEDGEMENTS

The work was funded by 'Central Innovation Program for small and medium-sized enterprises' (Federal Ministry for Economic Affairs and Energy, Germany), grant number: ZF4144918CL8. M. Jiang and J. Schmatz would like to acknowledge inspiring discussions with F. Wellmann (CGRE, RWTH Aachen University) on using the superpixel technology.

Open access funding enabled and organized by Projekt DEAL.

ORCID

Christiane Rößler Dr. rer. nat https://orcid.org/0000-0002-8420-4849
Florian Kleiner https://orcid.org/0000-0001-6002-0829

REFERENCES

1. Taylor, H. (1997). *Cement chemistry*. Thomas Telford Publishing. https://doi.org/10.1680/cc.25929
2. Scrivener, K. L. (2004). Backscattered electron imaging of cementitious microstructures: Understanding and quantification. *Cement and Concrete Composites*, *26*(8), 935–945. https://doi.org/10.1016/j.cemconcomp.2004.02.029
3. Rößler, C., Möser, B., & Ludwig, H.-M. (2017). Characterisation of microstructural properties of Portland cements by analytical scanning electron microscopy. *Cementitious materials: Composition, properties, application*, H. Pöllmann (Ed.). Berlin, Germany: De Gruyter. https://doi.org/10.1515/9783110473728
4. Möser, B., & Stark, J. (2003). High resolution imaging of wet building material samples in their natural state using Environmental Scanning Electron Microscope, South Africa: 11th International Congress on the Chemistry of Cement.
5. Stutzman, P. E., Bullard, J., & Feng, P. (2015). *Quantitative imaging of clinker and cement microstructure*. National Institute of Standards and Technology. http://doi.org/10.6028/NIST.TN.1877
6. Stutzman, P. E., Feng, P., & Bullard, J. W. (2016). Phase analysis of Portland cements by combined quantitative X-ray powder diffraction and scanning electron microscopy. *Journal of Research of the National Institute of Standards and Technology*, *121*, 47. https://doi.org/10.6028/jres.121.004
7. Pirrie, D., Power, M. R., Rollinson, G. K., Wiltshire, P. E. J., Newberry, J., & Campbell, H. E. (2009). Automated SEM-EDS (QEMSCAN®) Mineral Analysis in Forensic Soil Investigations: Testing Instrumental Reproducibility. *Criminal and environmental soil forensics*, K. Ritz, L. Dawson, D. Miller (Eds.). Dordrecht: Springer Netherlandsrlands. https://link.springer.com/chapter/10.1007/978-1-4020-9204-6_26
8. Gottlieb, P., Wilkie, G., Sutherland, D., Ho-Tun, E., Suthers, S., Perera, K., … Rayner, J. (2000). Using quantitative electron microscopy for process mineralogy applications. *Journal of the Minerals Metals and Materials Society*, *52*(4), 24–25. https://doi.org/10.1007/s11837-000-0126-9
9. Gu, Y. (2003). Automated scanning electron microscope based mineral liberation analysis: An introduction to JKMRC/FEI mineral liberation analyser. *Journal of Minerals & Materials Characterization & Engineering*, *02*(01), 33–41. https://doi.org/10.4236/jmmce.2003.21003
10. Schatten, H., & Pawley, J. B. (2008). *Biological low-voltage scanning electron microscopy*. New York, NY: Springer Science+Business Media LLC. https://doi.org/10.1007/978-0-387-72972-5
11. Georget, F., Wilson, W., & Scrivener, K. L. (2021). edxia: Microstructure characterisation from quantified SEM-EDS hypermaps. *Cement and Concrete Research*, *141*, 106327. https://doi.org/10.1016/j.cemconres.2020.106327
12. Heilbronner, R., & Barrett, S. D. (2014). Image analysis in earth sciences: Microstructures and textures of earth materials. *Lecture notes in earth sciences* (Vol. *129)*. Berlin, London: Springer
13. Stutz, D., Hermans, A., & Leibe, B. (2018). Superpixels: An evaluation of the state-of-the-art. *Computer Vision and Image Understanding*, *166*, 1–27. https://doi.org/10.1016/j.cviu.2017.03.007
14. Maitre, J., Bouchard, K., & Bédard, L. P. (2019). Mineral grains recognition using computer vision and machine learning. *Computers & Geosciences*, *130*, 84–93. https://doi.org/10.1016/j.cageo.2019.05.009
15. Tang, D., & Spikes, K. (2017). Segmentation of shale SEM images using machine learning. *SEG technical program expanded abstracts*. A. M. Popovici & S. Fomel (Eds.). Society of Exploration Geophysicists. https://library.seg.org/doi/10.1190/segam2017-17738502.1
16. Yu, J., Wellmann, F., Virgo, S., von Domarus, M., Jiang, M., Schmatz, J., & Leibe, B. (2021). Superpixel segmentations for thin sections: evaluation of methods to enable the generation of machine learning training data sets. Computer and Geosciences, in press. https://doi.org/10.31223/X55S65
17. Tian, X., & Daigle, H. (2018). Machine-learning-based object detection in images for reservoir characterization: A case study of fracture detection in shales. *The Leading Edge*, *37*(6), 435–442. https://doi.org/10.1190/tle37060435.1
18. Houben, M. E., Desbois, G., & Urai, J. L. (2014). A comparative study of representative 2D microstructures in Shaly and Sandy facies of Opalinus Clay (Mont Terri, Switzerland) inferred form BIB-SEM and MIP methods. *Marine and Petroleum Geology*, *49*, 143–161. https://doi.org/10.1016/j.marpetgeo.2013.10.009
19. Klaver, J., Desbois, G., Urai, J. L., & Littke, R. (2012). BIB-SEM study of the pore space morphology in early mature Posidonia Shale from the Hils area, Germany. *International Journal of*

Coal Geology, *103*, 12–25. https://doi.org/10.1016/j.coal.2012.06.012

20. Cosenza, P., Prêt, D., Fauchille, A.-L., & Hedan, S. (2019). Representative elementary area of shale at the mesoscopic scale. *International Journal of Coal Geology*, *216*, 103316. https://doi.org/10.1016/j.coal.2019.103316

How to cite this article: Jiang, M., Rößler, C., Wellmann, E., Klaver, J., Kleiner, F., & Schmatz, J. (2021). Workflow for high-resolution phase segmentation of cement clinker from combined BSE image and EDX spectral data. *Journal of Microscopy*, 1–7. https://doi.org/10.1111/jmi.13072